ELSEVIER

Journal of Structural Geology 27 (2005) 503–521

JOURNAL OF STRUCTURAL GEOLOGY

www.elsevier.com/locate/jsg

Combining natural microstructures with composite flow laws: an improved approach for the extrapolation of lab data to nature

M. Herwegh[a,*], J.H.P. de Bresser[b], J.H. ter Heege[c]

[a]*Institute of Geological Sciences, University of Bern, Bern 3012, Switzerland*
[b]*Department of Earth Sciences, Utrecht University, The Netherlands*
[c]*Institute for Geology, Mineralogy and Geophysics, Ruhr-University Bochum, Germany*

Received 5 February 2004; received in revised form 10 October 2004; accepted 20 October 2004
Available online 11 January 2005

Abstract

So far, rheological predictions that are based on experimentally derived flow laws appear inconsistent with microstructural observations in natural calcite mylonites because grain size sensitive (GSS) diffusion creep is predicted while microstructural criteria suggest grain size insensitive (GSI) dislocation creep as the dominant deformation mechanism. A way out of this discrepancy between experiment and nature can be found by combining full grain size distributions with composite GSS + GSI flow laws. We applied this approach to natural carbonate mylonites from the Helvetic Alps, Switzerland. For steady state microstructures, our calculations indicate an increasing GSS component with increasing temperature at geologically constrained strain rates of 10^{-10}–10^{-11} s^{-1}. The modeling results are consistent with microstructural observations of the natural mylonites: in these rocks, dynamically steady state microfabrics show a systematic change in grain size, grain size distribution and grain aspect ratio with temperature while crystallographic preferred orientations remain of similar strength. When single value mean grain sizes are used rather than grain size distributions, rheological modeling fails to give reasonable results. Further, paleostresses estimated from conventional recrystallized grain size piezometers were found to be unrealistically high, but were reduced to 80–100 MPa when results of the composite modeling were used. Hence, combining composite flow laws with microstructural data from natural mylonites forms a promising approach for a better extrapolation of experimental data to nature and therefore provides new insight into changes in rheology during large-scale geodynamic processes.

Keywords: Microstructure; Flow laws; Calcite mylonites

1. Introduction

Microstructures in naturally deformed rocks provide the crucial link between experimental rock deformation studies, microphysically based flow laws and deformation associated with large-scale tectonic processes. Among the large variety of crustal rocks, calcite aggregates are probably the most extensively studied, and a large body of data exists for both experimental and natural deformation at a wide range of conditions (see recent overviews by de Bresser et al. (2002), Renner and Evans (2002) and Renner et al. (2002)). At relatively high temperature (>400 °C), deformation conditions predicted on the basis of experimental work show reasonably good agreement with estimates from natural rocks (e.g. Busch and van der Pluijm, 1995; Ulrich et al., 2002). At low temperature, however, there is far less consistency. In particular, natural calcite rocks deformed at low temperature show ample evidence for grain size insensitive (GSI) dislocation mechanisms and associated dynamic recrystallization (e.g. Pfiffner, 1982; Burkhard, 1990; Kennedy and Logan, 1997), while extrapolation of experimental flow laws predict these rocks to be dominated by grain size sensitive (GSS) deformation mechanisms such as volume or grain boundary diffusion and grain boundary sliding accommodated by diffusion or dislocation processes (Brodie and Rutter, 2000; de Bresser et al., 2002). Indisputably, many problems exist with the comparison of natural observations to laboratory data (e.g. Paterson, 2001), but one important reason for the lack of consistency might

* Corresponding author. Tel.: +41-31-631-8764; fax: +41-31-631-4843
E-mail address: herwegh@geo.unibe.ch (M. Herwegh).

0191-8141/$ - see front matter © 2005 Elsevier Ltd. All rights reserved.
doi:10.1016/j.jsg.2004.10.010

lie in the uncertainties associated with the interpretation of microstructures in terms of creep mechanisms. The main focus of this paper is the interpretation of active creep mechanisms in pure calcite mylonites from the Helvetic Alps and the quantification of their contribution to the deformation in these rocks.

In recent years, extensive quantitative analysis of microstructures has become a standard part of rock deformation studies. Analyses have changed over the past decades from manual to computer-based techniques (e.g. Exner, 1972; Heilbronner and Bruhn, 1998; Herwegh, 2000), induced by the progress in computer soft- and hardware capabilities. This progress resulted in a change from 'number counting and lineal analysis' towards 'area scanning' methods. The latter have the advantage of allowing easy measurements to be made of the shape preferred orientation (SPO) of grains and the irregularity of grain boundaries in an aggregate, in addition to conventional grain size determination. This type of full quantitative analysis, supplemented by crystallographic preferred orientation measurement (CPO/texture, e.g. Adams et al., 1993; Panozzo et al., 1994; Fueten et al., 2002), is imperative for a non-subjective characterization of microstructural changes in both nature and experiment, ultimately aiming to determine the processes responsible for the observed changes. Examples of recent elaborate quantitative studies of highly strained calcite microstructures comprise the work of Molli et al. (2000), Bestmann et al. (2000) and Bestmann and Prior (2003) on natural rocks, and Pieri et al. (2001) and Barnhoorn et al. (2004) on experimentally deformed materials.

Concomitantly with the growing effort in extensive microstructure quantification of rock materials, more accurately defined mathematical relationships for grain growth, creep, and paleopiezometry have been developed. The full grain size distribution, including the distribution width, has been found to be potentially important in controlling creep behavior (Freeman and Ferguson, 1986; Handy, 1994; Heilbronner and Bruhn, 1998; ter Heege, 2002), but is not accounted for in the single-valued (mean) grain size approach normally applied in rock deformation. Small grains in a population may deform by other mechanisms than large grains in the same population (e.g. GSS and GSI, respectively), which holds for poly- as well as mono-mineralic aggregates. Consequently, rate equations are needed that combine different creep mechanisms for the same rock (Handy, 1994; ter Heege et al., 2004). As a first approximation, such composite rate equations can be built by combining two end-member flow laws, e.g. for GSI and GSS creep, using average (unimodal) grain sizes or explicitly including bimodal or multimodal grain size distributions (Raj and Ghosh, 1981; Wang, 1994). Freeman and Ferguson (1986) followed the approach of Raj and Ghosh (1981) and demonstrated by means of numerical methods that, in a general sense, the character of the distribution strongly influences the flow strength of a material deforming by multiple mechanisms. Ter Heege et al. (2002) specifically concentrated on the analysis of mechanical data and samples from experiments on calcite rocks (Carrara marble). Their application of composite flow behavior including grain size distributions resulted in predicted flow strengths that agreed well with measurements.

The present study tests the hypothesis that composite creep behavior constrained by quantified microstructural parameters can explain the apparent discrepancy between natural observations on deformed calcite rocks and predictions based on experiments. Although we focused on calcite, we believe that the approach is valid for other rocks as well.

Samples of this study are calcite mylonites from the Helvetic Nappe stack (Swiss Alps). The samples were taken from three major thrust planes and showed a systematic increase in deformation temperature in the range 250–380 °C. The shear zone width is in the range of 1–2 m. Geological constraints imply a strain rate along individual thrusts in the order of about 10^{-11} s^{-1}. As will be shown in Section 3.4, this information is important for the interpretation of the modeling results. Our approach consisted of: (1) microstructural analysis concentrating on quantifying the evolution and distribution of grain size, shape and orientation parameters, (2) calcite c-axis (texture) measurements, and (3) evaluation of laboratory derived flow laws against natural observations. The paper is organized along these steps.

2. Methods

2.1. Microfabric analysis

The hand specimens used in this study were all collected within large-scale thrust zones and were cut to cuboids with long axes parallel to the stretching lineation (nappe transport direction) and heights perpendicular to the rock foliation. Automatic quantification of grain cross-sectional areas using the program NIH image 1.62 was applied to determine for all samples: the average of the grain sizes (D), grain size distribution, grain aspect ratios (b/a) and grain shape preferred orientation (SPO). For this purpose, optical microscopy and electron backscatter imaging was performed on cuboid surfaces treated previously by two-step etching (for detailed information, see Herwegh, 2000) and digital grain boundary maps of the microstructures were created using the SEM and optical micrographs. The orientation of the X–Y plane used for measurements was always parallel to the stretching lineation and perpendicular to the foliation.

For grain size analysis, measured cross-sectional areas of grains were used to calculate equivalent circular diameters (ECD). In order to represent the data as grain size distributions, the frequencies of grains in intervals of fixed width (arithmetic scale) were determined, both on the basis

of the number of measurements (conventional number weighing, ECD_{nr}) and on the area fraction of the grains in the respective interval (area weighing, ECD_{area}). The latter method helps recognition of bimodal distributions. Distribution of log-normal and square root $ECD_{(ln,\ sqrt)}$ were determined in addition to $ECD_{(nr,\ area)}$. Independent of the chosen presentation pattern it is important to note that from a statistical point of view, data quality generally is good for classes of small grain sizes while it significantly decreases towards larger grains simply because of decreasing number of large grains per class. Being aware of this problem, different approaches exist to use the probability of sectioning effects in 2-D for an extrapolation towards 3-D (e.g. Wager, 1961; Heilbronner and Bruhn, 1998; Higgins, 2000). However, assumptions with respect to the 3-D grain shape have to be made. We used our data to determine the StripStar 3-D ECD_{ss} (Heilbronner and Bruhn, 1998). StripStar uses an adapted Schwartz–Saltykov method (see summary in Underwood, 1970), which calculates ECD_{ss} distributions based on comparison of the ECD_{nr} distributions with distributions of sectional circles generated by random intersection of a plane with a uniform distribution of spheres. An extensive treatise of the conversion of grain sections to volume fraction is beyond the scope of this paper, but see Underwood (1970) and Heilbronner and Bruhn (1998) for more details. StripStar data are essential for our analysis of the rheological behavior of the rocks under investigation (see Section 2.3 below). Mean grain sizes were calculated for all types of distributions, except for the ECD_{ss} for which the modes of the distributions were used.

For grain shape analysis, the grain boundary outlines were first digitized and then the orientation distribution function of b/a (minor/major grain axis) and the orientation α of the major axes with respect to the foliation were calculated with the program PAROR (Panozzo, 1983). To measure the convexity/concavity of grain surfaces the PARIS factor, as shape factor, was calculated with the program SHAPES (Panozzo and Hürlimann, 1983). In a more visual point of view, the PARIS factor quantifies the difference in length between a stretched rubber band wrapped around a grain and its actual surface, where with increasing degree of convexity/concavity, i.e. increasing lobateness, the PARIS factor increases. Hence, the PARIS factor gives information about the surface structure of a grain, which is important for detection and quantification of recrystallization mechanisms like grain boundary migration.

In order to visualize location dependent changes, the microstructural data of this study will be presented as a function of the inverse temperature.

2.2. Texture analysis

Texture (crystallographic preferred orientation/CPO) analysis was performed on ultrathin sections using the program GeoVision (GV) and an automatic rotation polarization stage (Fueten, 1997). Calcite C-axes were measured in two ways: (a) on nodes of an orthogonal grid with constant spacing for all samples, and (b) within the center of each grain. Approach (a) corresponds to area weighting while (b) is number weighted. The results were plotted and contoured on a stereographic projection with the computer program GEOrient 9.1 (Rod Holcombe). It is important to note that GV is not able to distinguish between C-axes with identical plunge but opposite trend (azimuth).

2.3. Rheological modeling

In order to compare geological constraints on deformation rates with constraints provided by flow laws, bulk differential stresses and relative contribution of GSS and GSI deformation were determined for the Helvetic calcite rocks at fixed strain rates. In our approach, state-of-the-art flow laws for GSS (diffusion, grain boundary sliding) and GSI (dislocation controlled) creep of calcite rocks were used (see Section 5), accounting for composite deformation mechanisms.

The GSS and GSI deformation mechanisms are assumed to contribute independently to the total strain rate, so that the total strain rate of grains in an individual grain size class (i) is given by $\dot{\varepsilon}_i = \dot{\varepsilon}_{GSS} + \dot{\varepsilon}_{GSI}$ (e.g. see Poirier, 1985, p. 79). Two types of calculations were performed: (I) using a single-valued grain size, i.e. the arithmetic mean from the relevant grain size distribution (hence applying only one grain size class) and (II) using the full grain size distribution (multiple classes). For the first method, an iterative approach was used comprising calculation of $\dot{\varepsilon}_{GSS}$ and $\dot{\varepsilon}_{GSI}$ for a range of stresses until a stress value was reached at which the total strain rate $\dot{\varepsilon} = \dot{\varepsilon}_{GSS} + \dot{\varepsilon}_{GSI}$ matched the geologically constrained strain rates. This method assumed the same stress to apply to both GSS and GSI mechanisms, taking the average value of the grain size as representative for the aggregate properties. We used this method to obtain a first impression of the relative importance of the GSS and GSI mechanism in our natural samples, by determining $\dot{\varepsilon}_{GSS}/\dot{\varepsilon}$. However, the single-valued grain size approach (I) does not account for the fact that individual rocks always show a range of grain sizes rather than a single value. The second method (II) provides a solution to this problem. We followed the procedure of ter Heege et al. (2002), which essentially involved two steps.

First, 2-D sectional areas were converted to 3-D volume fractions. The volume fractions (v_i) of grains within a certain grain size class (ECD_{ss}) were calculated from the number weighted distribution of grain cross-sectional areas (ECD_{nr}) using the program StripStar (Heilbronner and Bruhn, 1998).

Second, bulk strain rate or differential stress was calculated by volume averaging the strain rate/stress of grains in individual grain size classes. For the uniform stress end-member, grains in individual classes deform at a stress similar to the bulk stress. For an ECD_{ss} distribution with j

grain size classes, the bulk strain rate is given by:

$$\dot{\varepsilon}_\sigma = \dot{\varepsilon}_1 v_1 + \dot{\varepsilon}_2 v_2 + \ldots + \dot{\varepsilon}_j v_j = \sum_i \dot{\varepsilon}_i v_i \quad (1)$$

The bulk stress (σ) required to deform the calcite rock by a given strain rate ($\dot{\varepsilon}_\sigma$) was determined iteratively, and inserted in the composite flow law used to determine the strain rate of grains in individual classes ($\dot{\varepsilon}_i$). For the uniform strain rate end-member, grains in individual classes deform at a strain rate similar to the bulk strain rate. In this case, the bulk stress is given by:

$$\sigma_{\dot{\varepsilon}} = \sigma_1 v_1 + \sigma_2 v_2 + \ldots + \sigma_j v_j = \sum_i \sigma_i v_i \quad (2)$$

The stress (σ_i) required to deform grains in individual classes by a given strain rate ($\dot{\varepsilon}$) was determined iteratively for each class and inserted in Eq. (2) to give the bulk stress ($\sigma_{\dot{\varepsilon}}$). The relative contribution of GSS to the total deformation ($\dot{\varepsilon}_{GSS}/\dot{\varepsilon}$) was determined by volume averaging the strain rates of each grain size class resulting from the individual GSS and GSI mechanisms at the specific stress on grains within that class (i.e. σ, σ_i for uniform stress and uniform strain rate, respectively).

It should be emphasized that for the present approach to hold, two assumptions were implicitly made: (i) grain size is spatially non-correlated, i.e. there are no interconnected weak layers of fine grains or load-bearing frameworks of large grains, analogous to two phase materials with strong viscosity contrast between the phases (Handy, 1990) present, (ii) grain morphology is similar in the individual grain size classes. For the steady state microstructures used in the present analysis these two assumptions are not unrealistic (see Sections 4.2 and 4.3).

3. Geological setting

3.1. Tectonic framework and rock types

The area investigated is situated in the Helvetic Alps and is characterized by a nappe stack consisting of three major nappes, which are, from bottom to top: Doldenhorn, Gellihorn and Wildhorn nappes (Fig. 1). Nappe emplacement occurred during the Alpine orogeny during Early Oligocene to Miocene (Burkhard, 1988; Huon et al., 1994). The deformation sequence was heterochronous; Gellihorn and Wildhorn nappes were thrusted first during the Prabé phase (Burkhard, 1988) while the Doldenhorn nappe was emplaced later during the Kiental phase (Burkhard, 1988). The Helvetic nappe stack was exhumed during the Grindelwald phase (Burkhard, 1988; Pfiffner et al., 1997).

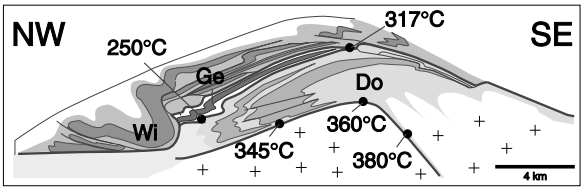

Fig. 1. Tectonic section through the area investigated. Do: Doldenhorn nappe, Ge: Gellihorn nappe, Wi: Wildhorn nappe.

According to Burkhard (1988) the original length dimensions of the nappes were 20, 6 and 12–15 km for the Wildhorn, Gellihorn and Doldenhorn nappes, respectively. The Wildhorn and Doldenhorn nappes show thicknesses of several kilometers, while the Gellihorn nappe is relatively thin, in the order of only a few hundred meters. Because of this low thickness and the fact that microstructural trends in the Gellihorn and Wildhorn nappes are identical, we treat these two nappes as one mechanical unit. Regarding final displacements, about 25 km was determined for the Gellihorn–Wildhorn nappes, while a minimum distance of 8 km was estimated from restoration of the Doldenhorn nappe. Emplacement of the Doldenhorn nappe underneath the existing nappe stack occurred at peak temperature metamorphic conditions inducing a short-term thermal overprint in the already overlying Gellihorn–Wildhorn nappes (Burkhard, 1988; Suchy et al., 1997; Arkai et al., 2002).

Mylonitic carbonate rocks are exposed along the basal thrusts of all three nappes. Two different types of original rocks that developed into carbonate mylonites were distinguished: (a) micritic limestones and (b) synkinematic veins. Especially in the Gellihorn–Wildhorn nappes, cyclic deformation behavior of veining and shearing occurred (see Herwegh and Kunze, 2002). Although locally still present, synkinematic veins are less abundant in the Doldenhorn nappe than in the other two nappes.

In the Doldenhorn nappe, late displacements at reduced temperatures induced very localized deformation under plastic and then brittle conditions. As a consequence, new microstructures developed in the center of the shear zone, which, however, can clearly be distinguished from those related to the major episode of thrusting. We excluded these late deformation microstructures from the analysis.

3.2. Temperatures and related errors

Peak temperatures are in the range from anchi- to epizonal conditions and increase from N to S as well as with increasing depth in the nappe stack (Fig. 1; Table 1). The reliability of geothermometers in this temperature range can be problematic (e.g. Frey and Robinson, 1999). For that reason, a combined approach of calcite–dolomite and calcite–graphite thermometry was applied. Calcite–graphite thermometry, performed on organic nano-scale flakes and matrix calcite, suggests a relative temperature increase of 40 °C from front to rear of the Doldenhorn nappe with an error of ± 5 °C. In terms of absolute temperatures, the obtained data are not reliable because of too severe

Table 1
Database of natural calcite mylonites. Ge/Wi: Gellihorn/Wildhorn nappes

Sample	Nappe	T (°C)	$1/T$ ($K^{-1}\times10^3$)	ECD_{nr} (μm)	ECD_{area} (μm)	ECD_{ss} (μm)	b/a	Angle α (°)
Do-8	Doldenhorn	345	1.62	6.68	10.7	11.4	0.68	4
Do-30	Doldenhorn	349	1.61	7.74	13.7	14	0.57	26
GS-126f	Doldenhorn	356	1.59	11.5	19.6	21.1	0.55	16
Do-26	Doldenhorn	361	1.58	15.7	32.4	35	0.67	2
Do-27	Doldenhorn	361	1.58	14.5	32.8	34.1	0.7	21
Do-28pure	Doldenhorn	361	1.58	12.43	23.7	25.5	0.57	8
Do-22	Doldenhorn	371	1.55	13.05	28.4	30	0.57	19
Do-24pure	Doldenhorn	371	1.55	13.47	27.4	26	0.44	18
Jung986.45D	Doldenhorn	379	1.53	23.47	40.6	39.8	0.36	0
Ge-3	Ge/Wi	250	1.91	1.63	2.5	2.68	0.8	14
Ge-6	Ge/Wi	250	1.91	2	2.97	3.34	0.69	24
Ge-8	Ge/Wi	315	1.7	3.41	5.38	5.62	0.92	26
Ge-9	Ge/Wi	313	1.71	2.74	5.14	5.44	0.69	7
Ge-10	Ge/Wi	307	1.72	2.43	4.19	4.43	0.94	10
Ge-11	Ge/Wi	303	1.74	1.7	2.65	2.84	0.86	37
Ge-12	Ge/Wi	298	1.75	1.94	4.5	3.37	0.7	18
Ge-13	Ge/Wi	265	1.86	1.9	3.05	3	0.85	6
Plam2	Ge/Wi	363	1.57	5.1	8.35	8.43	0.59	9
Wi-13	Ge/Wi	263	1.86	1.62	2.48	2.81	0.7	41
Wi-16	Ge/Wi	317	1.69	3.88	6.96	7.29	0.64	16
Wi-19	Ge/Wi	330	1.66	3.67	6.27	7	0.65	11

discrepancies between the individual geothermometers particularly for the low temperature range. Therefore, calcite–dolomite thermometry was additionally performed to recalibrate the calcite–graphite data indicating a temperature increase from 345 to 379 °C confirming the measured increase in relative temperatures by calcite–graphite thermometry. Regression of the calcite–dolomite data yields errors of ±25 °C. An additional error of at least ±10 °C is related to the position of the calcite solvus in the temperature range between 500 and 800 °C (this error might even increase towards lower temperatures; Anovitz and Essene, 1987). Most likely, the obtained temperatures represent maximum values, which correlate well with the predictions of Burkhard (1988).

For the Gellihorn–Wildhorn nappes, temperatures increased towards the south. Vitrinite reflectance data in the frontal part of the Wildhorn nappe suggested 160–180 °C (Burkhard and Kalkreuth, 1989), fluid inclusion thermometry in the central part of the Gellihorn nappe presented temperatures around 260 °C (Frey et al., 1980) and calcite–dolomite thermometry in the rear part of the Wildhorn nappe indicated temperatures as high as 350 °C (Burkhard, 1990). These values represent again maximum temperatures. Due to the thermal overprint mentioned above, the question could be asked if these temperatures are truly representative for the conditions during nappe emplacement. We found that the grain sizes of dynamically recrystallized calcite of the rear part of the Wildhorn nappe and the frontal part of the underlying Doldenhorn nappe are very similar, as will be demonstrated later. This suggests that these regions were deformed under similar conditions and that the impact of the late thermal overprint on the microstructure was limited. It is only manifest in a few samples with dynamically recrystallized calcite veins that show a slightly enhanced grain size compared with the mylonites originated from micrites. To avoid any bias in the data set, we excluded samples that showed remnants of a polymetamorphic history.

3.3. Time constraints on deformation

The major nappe emplacement in the investigated area took place in the time interval between 38 and 20 Ma (Burkhard, 1988). In case of the Gellihorn–Wildhorn nappe, K–Ar dating on very fine-grained micas revealed Alpine ages of 37.0±0.9 and 36.8±0.8 Ma (Huon et al., 1994). A maximum time interval of 38–28 Ma was assumed by Huon et al. (1994) for emplacement of the Gellihorn–Wildhorn complex. However, andesite clasts and biostratigraphic correlation of nanofossils (Ruffini et al., 1995) in the youngest foreland basin sediments (e.g. Taveyannaz sandstone), which were deposited before onset of any deformation in the mylonites, yield an age of 32–29 Ma. Despite these contradicting age determinations, the time span of 10 million years presents an upper bound for the duration of emplacement of the Gellihorn–Wildhorn nappe.

For the Doldenhorn nappe, Burkhard (1988) inferred a timing of thrusting between 30 and 20 Ma. This timing was confirmed by K–Ar dating on white micas that were recrystallized during thrusting (see also Herwegh and Jenni, 2001), yielding apparent ages of 28.5±0.7 Ma (Huon et al., 1994) and staircase $^{40}Ar/^{39}Ar$ time spectra with 32–13 Ma time limits for the beginning and ending of Ar-closure (Kirschner et al., 1996). Recent investigations on

regional metamorphism indicated that peak metamorphic conditions only lasted for 2–5 Ma (Arkai et al., 2002) and were closely related to nappe emplacement of the Doldenhorn nappe. Time constraints with respect to the end of thrusting are difficult to obtain, but post-tectonic telemagmatic quartzite dykes indicated a minimum age of 15.6 ± 0.7 Ma (Huon et al., 1994), however, not excluding earlier termination. Based on these considerations, 5 Ma seems to yield a realistic time period for emplacement of the Doldenhorn nappe but values of 2 and 10 Ma represent minimum and maximum estimations, respectively.

3.4. Strain rates and related errors

We have investigated the shear strain rate for the calcite mylonites under the assumption of simple shear and using constraints on the amount of displacement, width and time of activity of the shear zones bounding the nappes. To a first approximation, the assumption of simple shear is reasonable for high strain zones of limited width in the meter range in comparison to a total displacement of several kilometers. For both the Doldenhorn and Gellihorn–Wildhorn nappes, the thickness of the carbonate mylonite generally does not exceed 20 m and usually is in the range of 1–5 m (mostly <2 m), while total displacements might be as high as 25 km (Section 3.1). Deformation in the footwall is limited for both the Gellihorn–Wildhorn and the Doldenhorn nappes. The largest part of the thrust plane of the latter nappe is situated right on top of the more rigid rocks of the crystalline basement, drastically reducing the capability of strain accommodation in the footwall. This is different in the slates of the footwall of the Gellihorn–Wildhorn nappes. However, syndeformational calcite veins are much less deformed in the slates than in the thrust plane indicating that footwall deformation during thrusting was only able to accommodate a limited amount of strain. In a geodynamic context, the strain rates of the different nappes must be situated in a similar range. Using the estimated displacements and the most reasonable time constraints (Fig. 2), and considering only strain rates from overlapping parts of the suggested ranges for both nappes, relatively fast shear strain rates in the range of 8×10^{-12}–2×10^{-11} s^{-1} resulted (Fig. 2). If we take into account the uncertainties in shear zone thickness and timing (gray bars in Fig. 2), the range of possible shear strain rates expands, but strain rates slower and faster, respectively, than 3×10^{-12} s^{-1} and 1×10^{-10} s^{-1} can be excluded.

Our estimations can be compared with plate convergence rates between Europe and Africa for the appropriate time interval to assess the reliability of the shear strain rate estimations. Using the location of the Doldenhorn nappe, a section with strike 147° and rotation poles of Royer (1992), Ricou (1994) and Rosenbaum et al. (2002), average convergence rates of 0.9 cm/a result (Buiter, pers. commun.). This value converts to strain rates of 10^{-11}–10^{-10} s^{-1}, if 1–20-m-wide shear zones are taken into account. The comparison reveals that shear strain rates between 10^{-11} and 10^{-10} s^{-1} seem reasonable, while slower strain rates deviate from the plate tectonic constraints. Note that although seemingly fast, strain rates in the obtained range are not unusual and have been documented for other upper crustal shear zones (Pfiffner and Ramsay, 1982). They are probably the norm in the mid-upper crust.

4. Results—microstructures

4.1. On the way to steady state grain sizes

The occurrence of two different types of calcite starting material, namely (a) coarse-grained synkinematic vein calcite and (b) fine-grained micritic limestones, in combination with temperature gradients along the thrust planes provided a unique opportunity to investigate the evolution towards a steady state grain size for different starting grain sizes and different temperatures in a natural environment. The evolution is visualized in Figs. 3 and 4.

(a) Irrespective of the temperature, vein calcite became intensively twinned after precipitation (Fig. 3a and e). The ability of twinning to accommodate strain is limited and

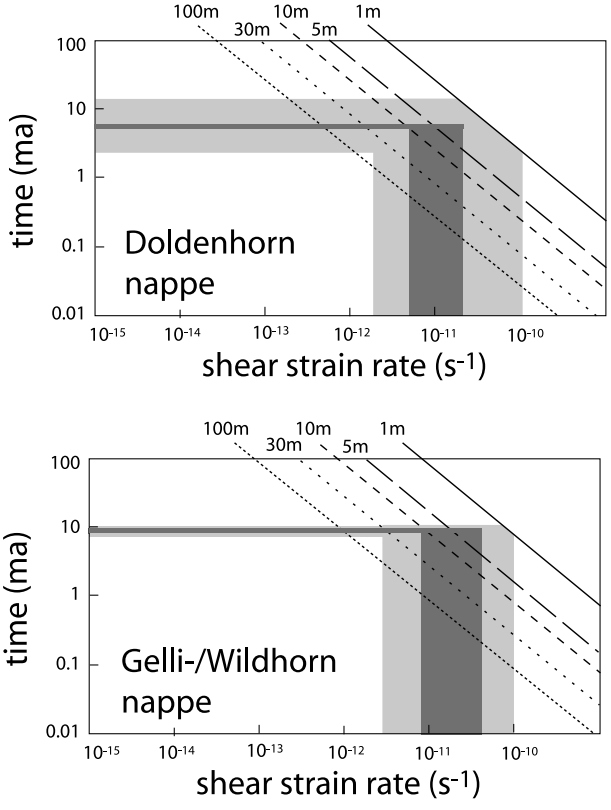

Fig. 2. Strain rate estimations for different shear zone widths assuming continuous simple shear deformation. Based on radiometric age constraints (vertical axis) and the inferred shear zone widths the shear strain rates most likely (dark gray) and the maximum possible range (bright gray) can be estimated for the Doldenhorn (top) and the Gellihorn–Wildhorn (bottom) nappes.

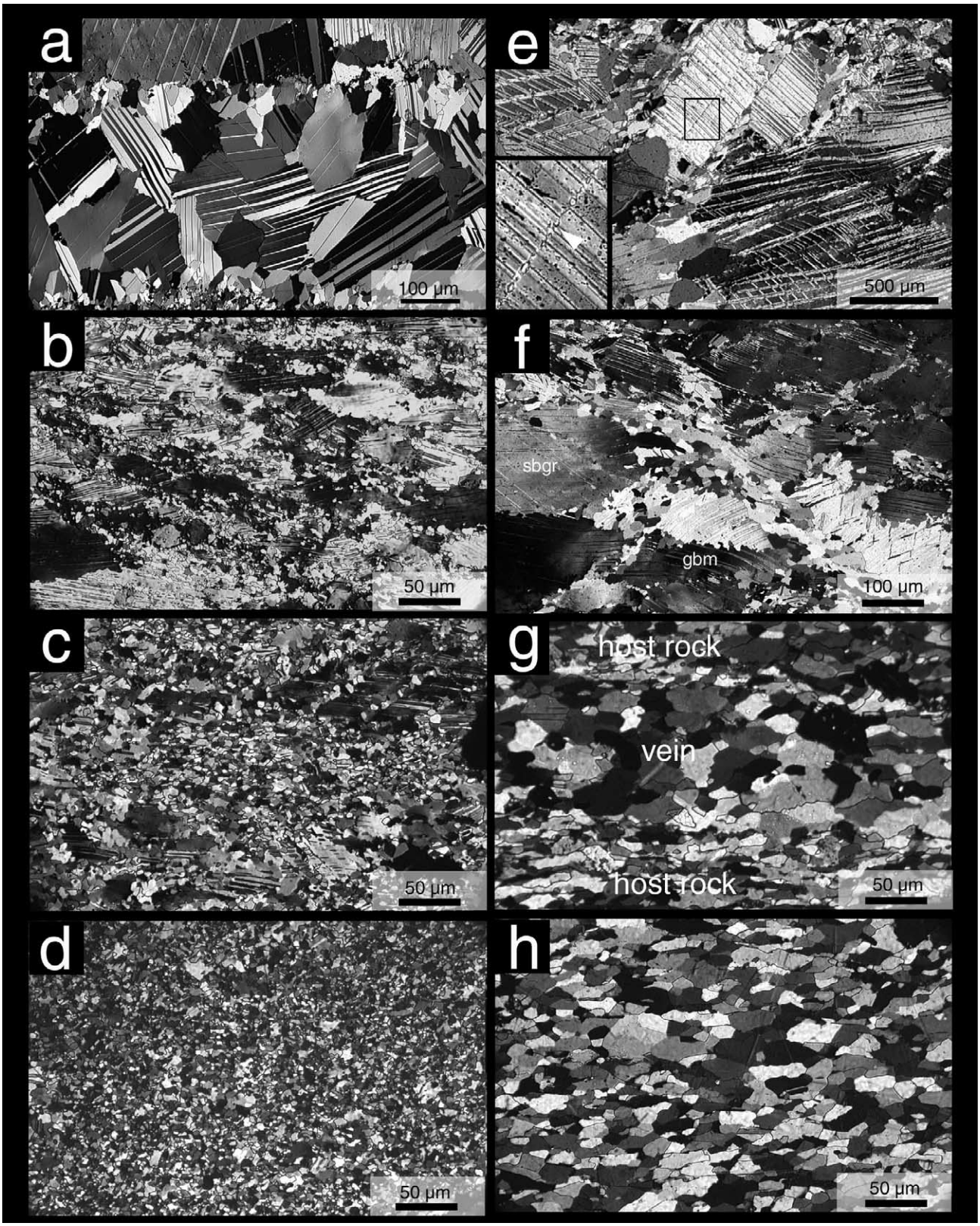

Fig. 3. Grain size reduction sequence in vein calcite of the Gellihorn/Wildhorn (left column Ge-3) and Doldenhorn (right column Do-28) nappes starting from intensively twinned aggregates (a, e). With increasing deformation, the amount of recrystallized grains increases at moderate shear strains (b, f) until a completely recrystallized matrix remains (c, g). Note that grain size reduction occurs by a combination of brittle deformation, spontaneous nucleation (e and inset in e), subgrain rotation recrystallization (sbgr) and grain boundary migration recrystallization (gbm, e.g. f). (d, h) Show deformation microstructures that developed from the original micritic protolith at the same locations (samples Ge-6 and Do-8). Note the resemblance between c, d and g, h.

other mechanisms were activated to allow continued straining of the vein calcite. The initially large grains were dissected by fracturing and small grains nucleated along the fracture planes by spontaneous nucleation (Fig. 3e and inset). Further straining of the calcite lattice of larger vein calcite fragments induced subgrain rotation recrystallization and migration of twin boundaries, which both supported the formation of relatively small new grains. Finally, bulging nucleation also contributed to the creation of new grains. With ongoing deformation, the amount of fine-grained recrystallized matrix continuously increased and therefore only few small remnants of the host grains persisted at high strains (Fig. 3c and g). As a consequence of this deformation history, the grain size distribution changed from a broad unimodal pattern in the weakly deformed state (original vein) to a bimodal grain size distribution at moderate shear strains (partly recrystallized vein; Fig. 4). Towards high strain, the bimodal distributions transformed again into a unimodal pattern (near-completely recrystallized vein), by strengthening the peak that reflects small grain sizes. Note that this deformation sequence is rather common in upper-mid crustal calcite rocks and was found in other orogens as well (e.g. Kennedy and Logan, 1997; Kennedy and White, 2001).

(b) In the case of former micritic limestones, the grain size continuously increases with increasing temperature, pointing to grain growth as the major microstructure modifying process (Figs. 3d and h and 4). More importantly, the mean grain sizes of the modified micrite and that of the recrystallized vein calcite are very similar and show the same change with temperature (see also Table 1). Hence, different starting materials (coarse-grained veins and fine-grained micrites) recrystallized to the same dynamical steady state grain size. Although we focused in this study exclusively on micritic microstructures with no or only minor amounts of micron-scale second phases, in the same rock types the second phase content can be as high as 15 vol%. For those second phase sheet silicates, Herwegh and Jenni (2001) showed an increase in grain size with temperature, which, however, is less pronounced than for calcite.

4.2. Quantification of grain parameters

Grain size distributions can be characterized using

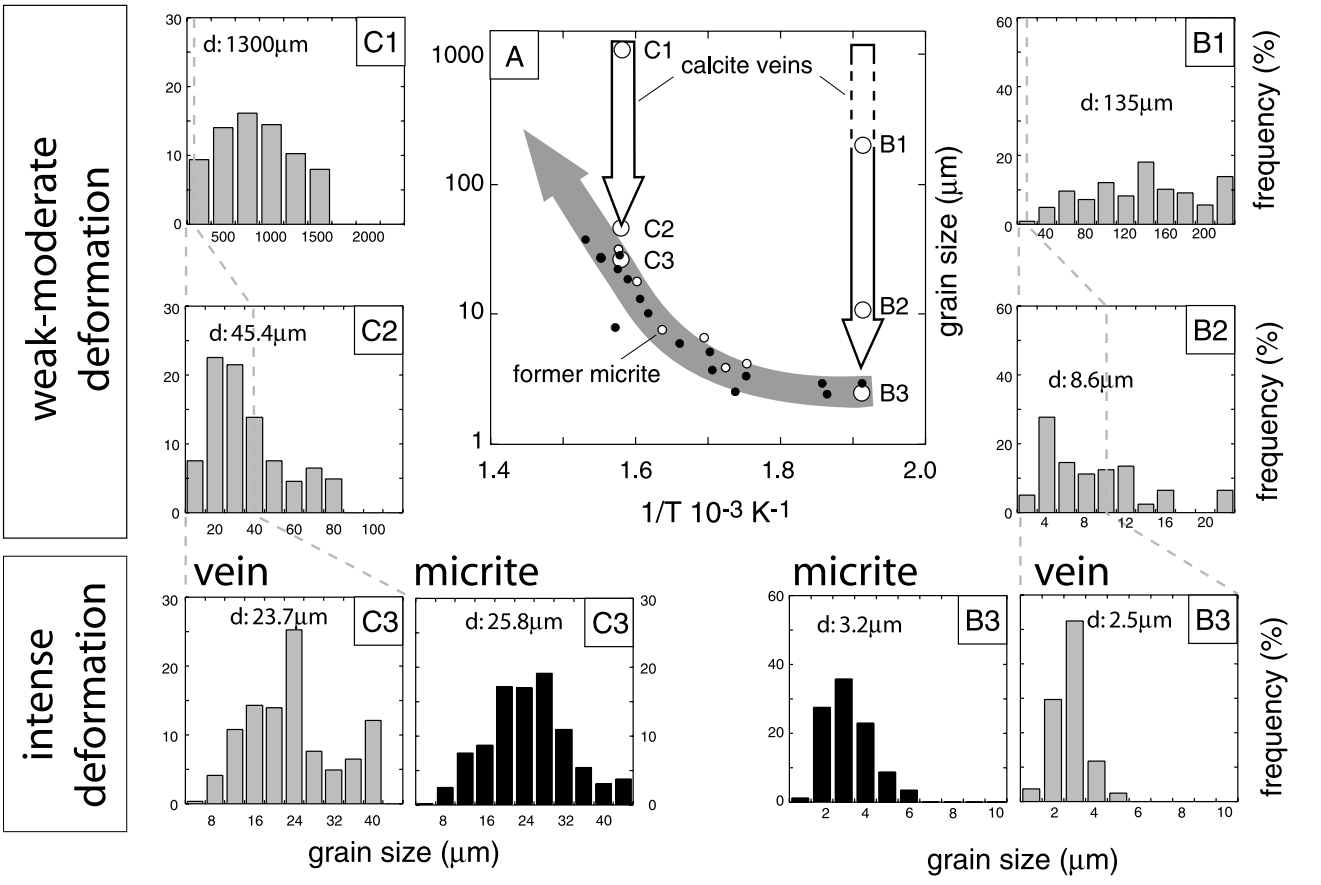

Fig. 4. Grain size evolution for vein calcite and former micrite as a function of the inverse temperature for all samples (A). Note that with increasing strain, mean grain size and distribution of vein calcite change resulting in a fine-grained steady state microstructure with similar grain size as observed in the former micrites (see B3, C3). Steady state grain size increases in both deformed micrite (dark circles) and deformed vein calcite (white circles) with increasing temperature.

parameters such as skewness and kurtosis (Fig 5). The symmetry of the distribution pattern depends on the chosen interval of the grain size classes (Fig. 5a). Skewness data of ECD_{nr} (mean value 1.02 ± 0.28) show the most intense skewness while this continuously decreases from right skewed $ECD_{area}(0.50 \pm 0.37)$, $ECD_{sqrt}(0.31 \pm 0.21)$ and $ECD_{ss}(0.36 \pm 0.49)$ to left skewed ECD_{ln}, (-0.44 ± 0.25). A skewness of zero would represent a symmetric distribution and therefore none of the obtained distributions is entirely symmetric. However, the deviations for ECD_{area}, ECD_{sqrt}, ECD_{ss} and ECD_{ln} are in a limited and similar range, suggesting that mean and median values of the distributions are nearly identical. The skewness remains constant with increasing temperature (Fig. 5a). For the selected distribution patterns the kurtosis is close to zero supporting the previously gained information of grain size distributions with only slight asymmetry (Fig. 5b). The kurtosis increases with increasing temperature. As a function of the inverse temperature, both median grain size (ECD_{ln}) and the corresponding standard deviation of the grain size distribution increase in a nonlinear way (Fig. 6).

In terms of SPO, the aspect ratio of the grains in the Gellihorn–Wildhorn and Doldenhorn nappes is between 0.6 and 0.95, and 0.4 and 0.7, respectively, and therefore decreases with increasing temperature (Fig. 7; Table 1). The average orientations (α) of the grain major axis are roughly in the range of 5–30°, indicating only weak to moderate inclinations with respect to the shear plane (Table 1). SPO angle α slightly decreases with temperature. The PARIS factor increases with increasing temperature, but, similar to the median values, shows a stronger increase per temperature interval at high temperatures, i.e. in the Doldenhorn nappe (Fig. 8). In this way PARIS values cover a range from 3 to 9%.

4.3. Steady state textures (CPO)

The CPO of all analyzed samples are characterized by c-axis point maxima, which are oriented perpendicular to the shear plane. All patterns derived from high strain samples are completely dynamically recrystallized and are therefore interpreted to represent steady state microfabrics. Only a few of the patterns show a slight asymmetry (Fig. 9; see also fig. 6 in Herwegh and Kunze, 2002). This type of c-axis pattern is commonly observed in carbonate shear zones (Schmid et al., 1981; Dietrich and Song, 1984; Lafrance et al., 1994; Bestmann et al., 2000). No change in texture intensity or c-axis pattern as function of temperature is observed for the temperature range investigated (Fig. 9). EBSD analysis of Herwegh and Kunze (2002) revealed that a-axes are dispersed along a great circle parallel to the shear plane (see their fig. 6).

5. Results–rheology

The rheological behavior of the mylonites from the Helvetic Nappe stack has been assessed allowing for multiple deformation mechanisms (GSI+GSS). The method employed has been outlined above (Section 2.3). For dislocation (GSI) creep, the dislocation cross slip controlled creep equation for marble of de Bresser (2002) was taken (Table 2). This law has the mathematical form of an exponential creep equation, which has been shown to fit experimental calcite data better (i.e. over a wider range of deformation conditions) than the more conventional Dorn-type power law (see Renner and Evans, 2002). For GSS flow, both the creep equation of Walker et al. (1990) and the more recently published rate equation by Herwegh et al. (2003) have been tested (Table 2). Both GSS equations are based on experimental deformation of synthetic calcite aggregates, but differences in character of the materials

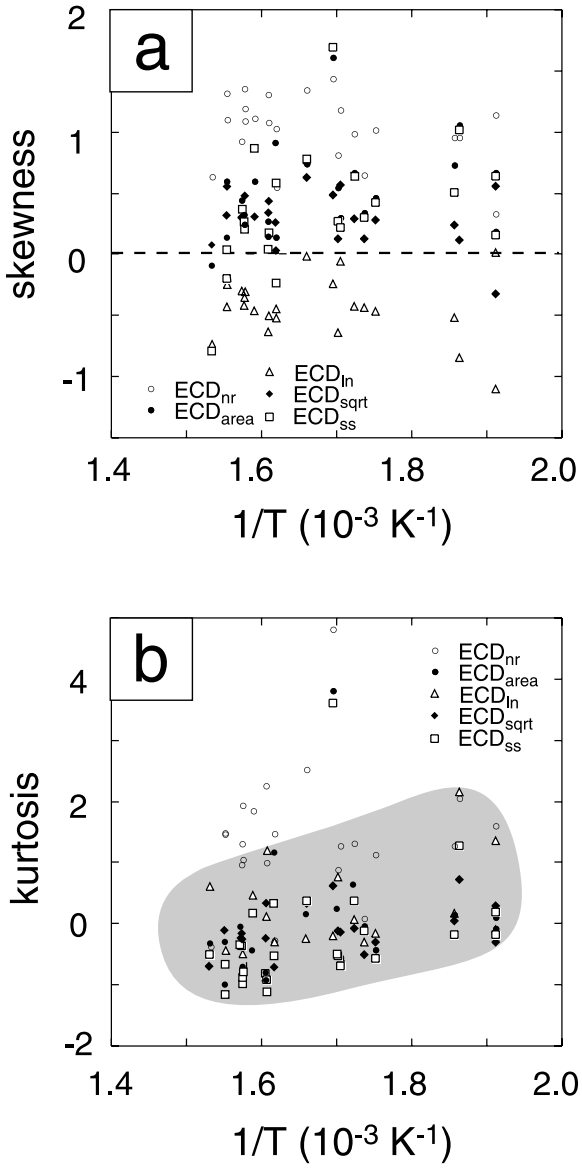

Fig. 5. Skewness (a) and kurtosis (b) of the samples as a function of inverse temperature T using different methods for the presentation of grain size distributions.

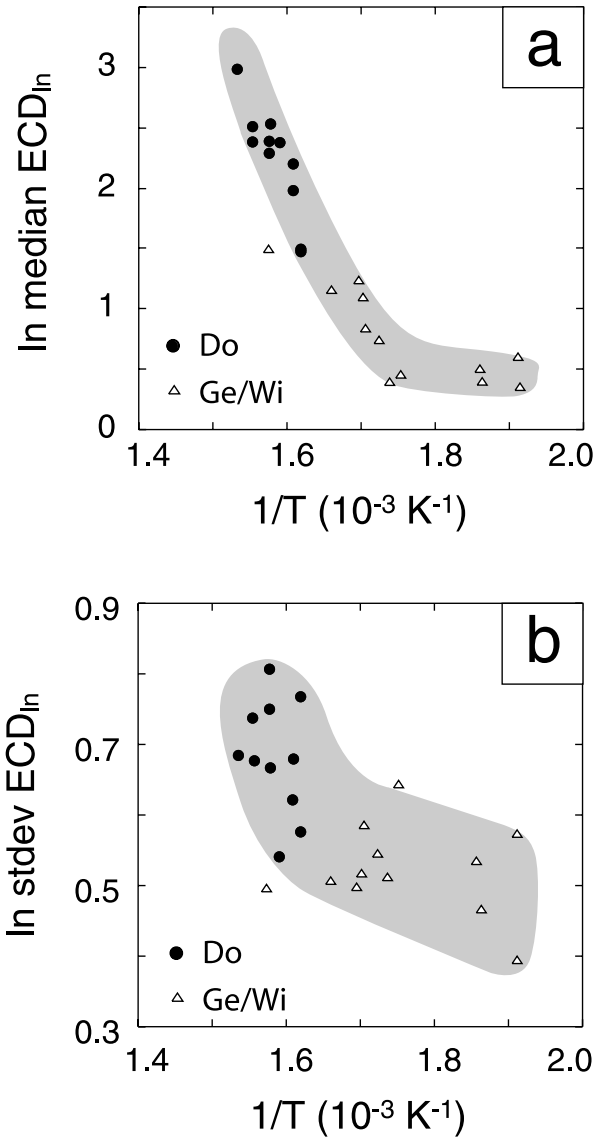

Fig. 6. Increase in ln median (a) and ln standard deviation (b) of the grain size distributions as a function of the inverse temperature T for the Doldenhorn (Do) and the Gellihorn/Wildhorn (Ge/Wi) samples.

resulted in strain rate–stress relations that differ substantially. The relationship from Walker et al. (1990) represents the weaker material. First, GSS creep laws including a single-valued (i.e. average) grain size were combined with the GSI creep law. The resulting composite creep equation was evaluated for strain rates of 10^{-12}, 10^{-11} and 10^{-10} s^{-1}, covering the range of relevant strain rates for the Helvetic mylonite samples (Fig. 2). We also carried out calculations for a strain rate of 10^{-9} s^{-1}. This relatively fast rate appears not very relevant for our natural samples, but helps visualizing trends in the data. The results are shown in Fig. 10, where the percentage of GSS contribution to the overall creep rate (i.e. $100[\dot{\varepsilon}_{GSS}/(\dot{\varepsilon}_{GSS}+\dot{\varepsilon}_{GSI})]$; see Section 2.3) is plotted as a function of reciprocal deformation temperature. When the Walker et al. (1990) rate equation for

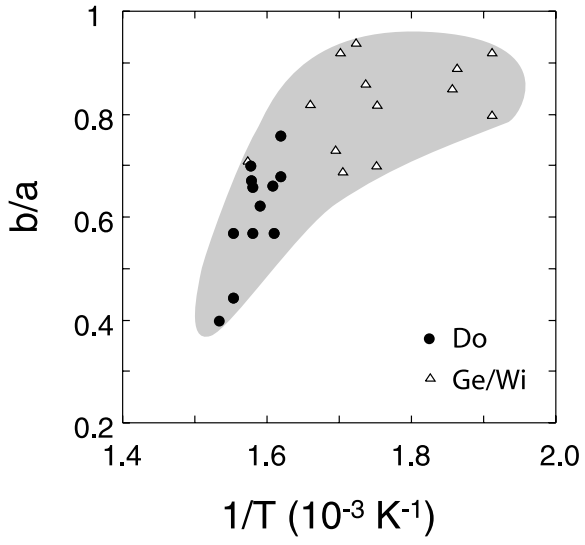

Fig. 7. SPO: decreasing grain aspect ratio (minor/major axis = b/a) with increasing temperature indicating increasing grain elongation with T.

GSS creep (Table 2) was applied, the calculations suggested that almost all Helvetic samples have been deformed dominantly, or even exclusively, by diffusion creep mechanisms (Fig. 10a–c). Only for the (unrealistic?) fast strain rate of 10^{-9} s^{-1} the calculated contribution of GSI mechanisms appears consistent with the ample microstructural evidence for active dislocation mechanisms (e.g. Fig. 9). Using the GSS rate equation of Herwegh et al. (2003), deformation of the natural samples is expected to have been dominated by GSS if strain rate was 10^{-12} s^{-1} (Fig. 10f), combined GSI + GSS if $\dot{\varepsilon}$ was 10^{-11}–10^{-10} s^{-1} (Fig. 10e), and exclusively GSI at 10^{-9} s^{-1} (Fig. 10d). However, the values for the %GSS of total creep rate do not show any systematic dependence on deformation temperature—they are scattered through the diagrams.

Subsequently, full grain size distributions rather than single mean values have been used to calculate the GSS contribution to the overall creep rate (Fig. 11). In this approach, small grains in the distribution contribute in

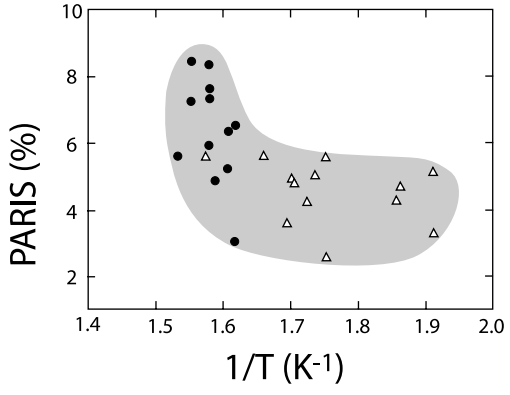

Fig. 8. Grain surfaces: PARIS factor increases with increasing T. Note that an increasing PARIS indicates an increasing convexity/concavity.

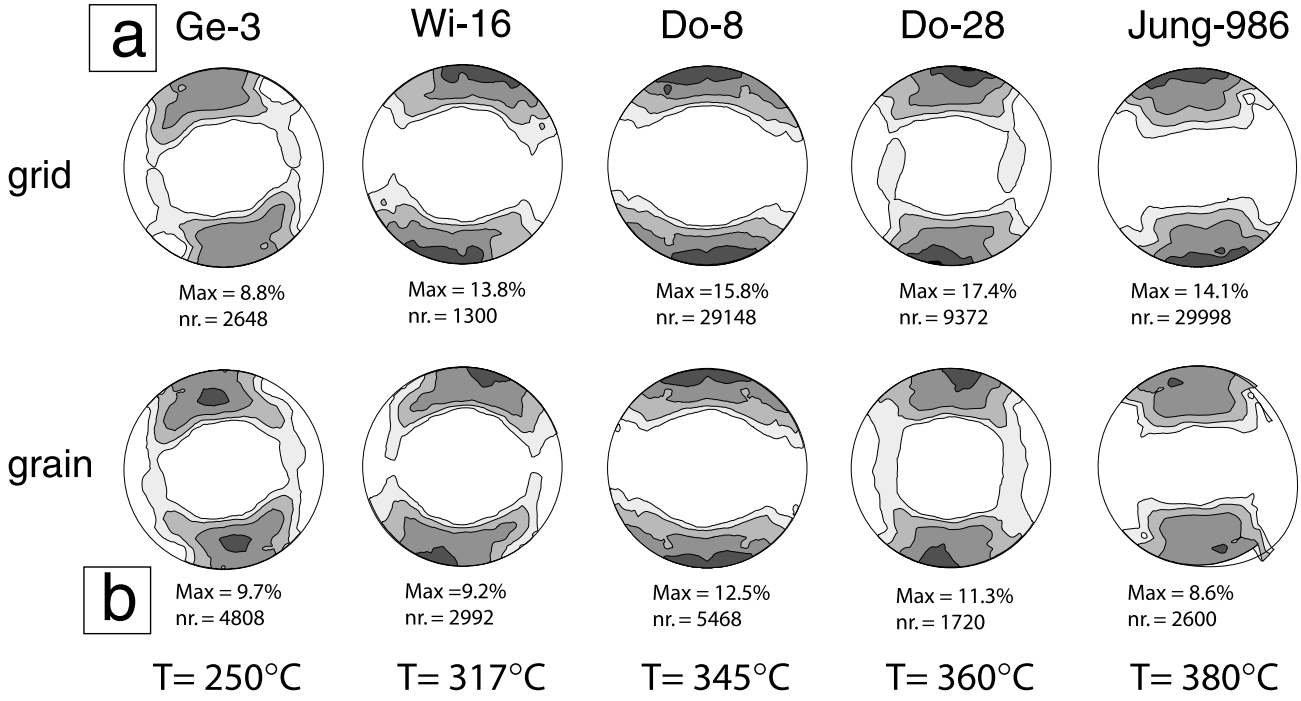

Fig. 9. CPO: c-axis patterns based on grid node measurements (a) and measurements in the center of each grain (b) for selected samples representing area and number weighted data sets, respectively. Contour intervals are 1, 2, 4… times uniform distribution.

another way to the overall creep behavior than large grains, while the single value method (Fig. 10) cannot make that distinction. Note that we performed our analysis assuming that stress or strain rate was distributed homogeneously through the aggregate (Section 2.3). After applying both the Walker et al. (1990) and Herwegh et al. (2003) rate equation for GSS, three important points emerged:

- at all individual strain rates tested, the role of GSI is more prominent if grain size distributions rather than single values are used in the calculations (cf. Figs. 10 and 11);
- for the conditions under consideration, application of the Herwegh et al. (2003) rate equation for GSS predicts lower %GSS of total rate than would come out if Walker et al. (1990) are followed (Fig. 11a–d vs. Fig. 11e–h);
- calculations including grain size distributions result in a general trend of increasing %GSS to bulk deformation with increasing temperature.

These general observations are independent of whether homogeneous stress or homogeneous strain rate was assumed.

6. Discussion

A great advantage of the chosen field laboratory with fine-grained mylonitic limestones and coarse-grained syn-deformational veins is that microstructural evolution at individual localities could be studied as a function of relative increase in shear strain at constant temperature. Further, by comparing samples from different outcrops of the same mylonite zone, deformed at potentially similar strain rate, temperature dependent changes in both microstructural evolution and steady state microfabrics could be investigated. In the following sections we will first discuss strain-dependent microstructure evolution in relation to mechanisms of (transient) deformation (Section 6.1) and then focus on temperature-dependent microstructural changes during steady state deformation (Section 6.2). We continue by evaluating the relative contribution of the deformation mechanisms using the microstructural results for steady state and the calculations of composite creep (Section 6.3). Finally, we compare estimates on paleostresses derived from our rheology modeling with values that can be obtained applying conventional recrystallized grain size piezometry (Section 6.4).

6.1. Deformation mechanisms during transient stages

In the present field area, the recurrent supply of coarse-grained vein calcite during the rock history and type and amount of deformational overprint (e.g. location and amount of recrystallization) allowed different but successive transient stages of vein deformation to be recognized. In the first transient stage, vein calcite was deformed by pervasive mechanical twinning during initial straining. During the second transient stage, deformation was strongly localized by microshearing, either along pre-existing anisotropies like grain and twin boundaries or along newly formed fractures.

Table 2
Calcite flow laws used for calculations

#	Flow law	Parameters used	Type	Reference
1[a]	$\dot{\varepsilon} = K\left(\frac{\sigma}{\mu}\right)^2 \exp\left[-\frac{\Delta U_{cs}\left(1-\frac{\alpha b\sigma}{\gamma}\right)}{kT}\right]$	$\mu = \mu_0 - 9.7T$	GSI, dislocation cross slip controlled	de Bresser (2002)
	$\Delta U_{cs} = \left(\frac{\mu b^3}{1859(\gamma/\mu b)}\right)\left(\ln\left[\frac{2\sqrt{3}}{16\pi(\gamma/\mu b)}\right]\right)^{0.5}$	$\mu_0 = 34180$ MPa		
		$b = 6.37\times10^{-10}$ m		
		$\alpha = 2.18$		
		$\log K = 6.90$		
		$\gamma = 0.192$ J m^{-2}		
2[b]	$\dot{\varepsilon} = A\sigma^n d^m \exp\left[-\frac{Q}{RT}\right]$	$n = 1.1$	GSS, grain boundary diffusion/ sliding	Herwegh et al. (2003)
		$m = -3.3$		
		$Q = 200$ kJ mol^{-1}		
		$\log A = 7.63$		
3[b]	$\dot{\varepsilon} = A\sigma^n d^m \exp\left[-\frac{Q}{RT}\right]$	$n = 1.7$	GSS, grain boundary sliding[c]	Walker et al. (1990)
		$m = -1.87$		
		$Q = 190$ kJ mol^{-1}		
		$\log A = 4.93$		

$\dot{\varepsilon}$ is strain rate, σ is stress, R is the gas constant, k is Boltzmann constant, and T is temperature (in K).

[a] In the cross slip controlled flow law, $\Delta u_{cs}(\sigma)$ is a stress dependent activation energy, μ is the (temperature dependent) shear modulus, b is the Burgers vector length, α and K are constants, and γ is the stacking fault energy. For details consult de Bresser (2002).

[b] Conventional Dorn-type power law with stress independent activation energy Q, dimensionless constants n and m, and constant A in MPa^{-n} μm^{-m}.

[c] Grain boundary sliding accommodated by volume diffusion and dislocation processes.

Within this transient stage, grain size was drastically reduced by a combination of fracturing, subgrain rotation recrystallization, bulging nucleation, twin- and grain boundary migration, and spontaneous nucleation of new grains via dissolution–precipitation processes. In the third transient stage, deformation became more homogeneous (i.e. no microshearing) as the amount of fine-grained vein calcite increased and only few remnants of the former coarse-grained calcite persisted.

We may compare the above sequence of transient stages in (initially) coarse-grained vein calcite with the results of high strain experimental deformation of calcite (notably,

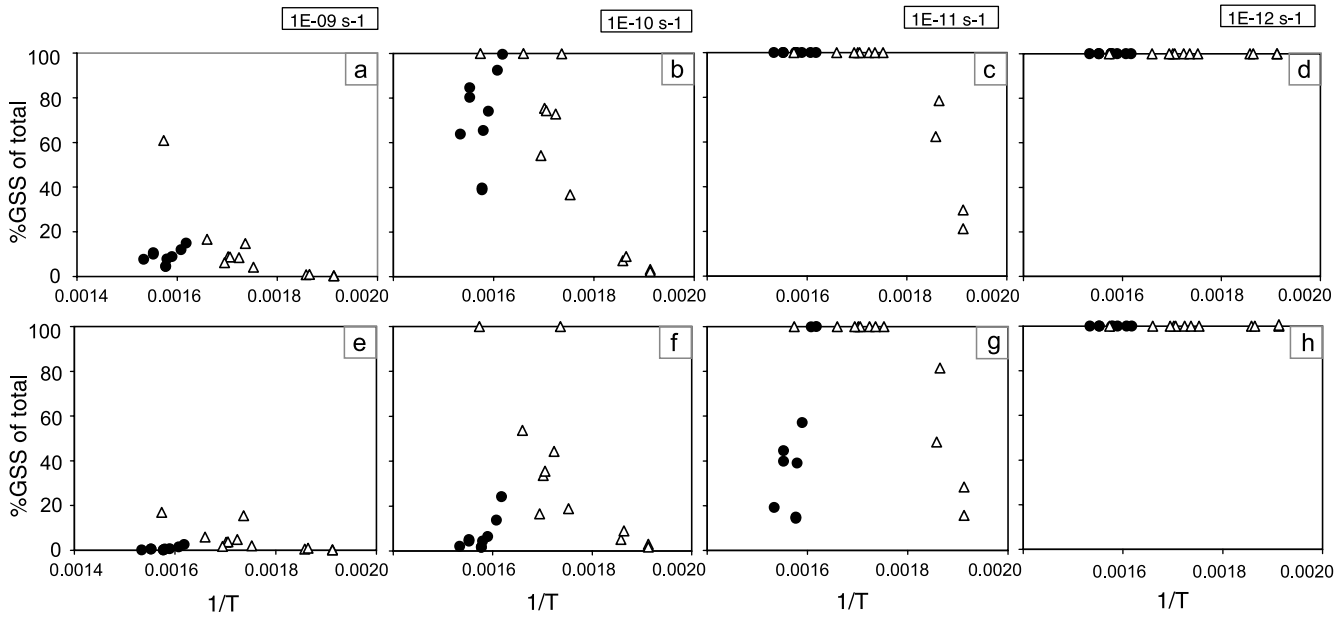

Fig. 10. Results of rheology modeling using mean grain sizes determined for the natural samples (Ge/Wi: triangles, Do: circles) and applying the dislocation cross slip controlled creep equation of de Bresser et al. (2002) and the diffusion creep equations of Walker et al. (1990), (a)–(d) or Herwegh et al. (2003), (e)–(h). Vertical axis indicates relative contribution to total of the grain size sensitive creep component.

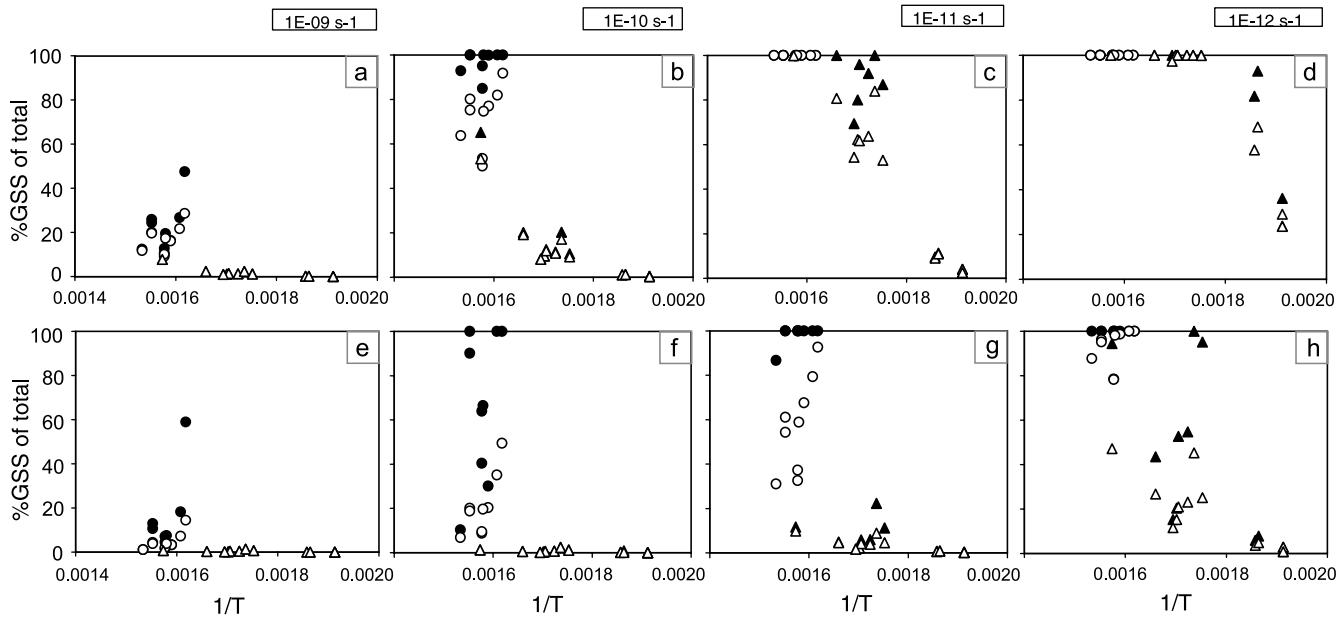

Fig. 11. Results of rheology modeling using grain size distributions of the natural samples (Ge/Wi: triangles, Do: circles) and applying the dislocation cross slip controlled creep equation of de Bresser et al. (2002) and the diffusion creep equations of Walker et al. (1990), (a)–(d) or Herwegh et al. (2003), (e)–(h) at homogenous stress (closed symbols) or strain rate (open symbols). Vertical axis indicates relative contribution to total of grain size sensitive creep component. For some data points, the values for homogenous stress and homogeneous strain rate overlap.

Carrara marble: Schmid et al., 1987; Pieri et al., 2001; ter Heege et al., 2002; Barnhoorn et al., 2004). The first stage (twinning) correlates well with the low strain part of experiments on Carrara marble. The second stage, however, comprised simultaneous occurrence of fracturing, mass-transfer processes and spontaneous nucleation, which has not been described for experiments on calcite rock deformed to intermediate strain. Most likely, these processes are not active in deformation experiments, because these experiments are generally performed at much higher temperatures than calculated for the investigated Helvetic nappe stack and the fluid conditions are probably incorrect for calcite dissolution and precipitation (e.g. Caciagli and Manning, 2003). The third stage on the other hand corresponds well with the ductile high strain part of experiments (see in particular Pieri et al., 2001 and Barnhoorn et al., 2004). In a broad sense, the experiments show a strain-dependent change in relative contribution of individual deformation mechanisms to the overall creep, which is comparable with the three successive stages of progressive deformation of natural vein calcite. Ter Heege et al. (2002) showed that rheological changes during transient high temperature deformation of Carrara marble can be explained by an increase of the relative contribution of GSS deformation due to grain size reduction during dynamic recrystallization. Therefore, rheological changes during shear zone evolution can be monitored by analyzing the grain size distribution of rocks with microstructures produced during the individual transient stages and applying a composite flow law based on the relevant GSS and GSI deformation mechanisms. Full analysis of the rheological changes during all of the stages associated with the low temperature evolution of the vein calcite studied is hampered by the difficulties in quantification of the relative contribution of other processes, such as brittle and mass transfer processes. Furthermore, the effect of evolving CPO (e.g. Pieri et al., 2001; Barnhoorn et al., 2004) would not be taken into account with a sole grain size dependent approach.

6.2. Deformation mechanisms during steady state

Our observations indicate that both micritic limestones and calcite veins evolve towards the same average grain size (Fig. 4). We interpret this as a characteristic dynamic steady state grain size, maintained by a balance between grain size reducing/nucleation and grain growth processes (see also Means, 1981; Karato, 1989; Herwegh et al., 1997; Shimizu, 1998; de Bresser et al., 2001). The occurrence of a steady state grain size, together with well developed CPO and SPO, is in good agreement with the results of many previous studies on calcite mylonites deformed under similar natural conditions. Kennedy and Logan (1997) and Kennedy and White (2001) suggested for similar microstructures as discussed here, that deformation in vein calcite occurred first by GSI and then, when dynamic recrystallization resulted in a substantially reduced grain size, by GSS accompanied by GSI. In their case, the micritic protolith to the mylonite did not show grain growth. In most other studies of deformed calcite rocks, microstructures of the type of the Helvetic mylonites have been interpreted to indicate deformation well within the dislocation creep field (Pfiffner, 1982; Heitzmann, 1987; Burkhard, 1990; Van der

Pluijm, 1991; Busch and van der Pluijm, 1995; Badertscher and Burkhard, 2000; Bestmann et al., 2000; Molli et al., 2000; Ulrich et al., 2002). This interpretation, however, does not account for the fact that continuous reworking of the microstructure by grain size reduction and growth results in a range of grain sizes being present at any time during the deformation history, allowing for the possibility that small grains deform by different mechanisms than large grains in the same aggregate. In particular, mass transfer/diffusion processes need to be considered, since these strongly depend on grain size and potentially govern deformation in addition to dislocation mechanisms. Some aspects of our microstructural observations specifically point to diffusion processes and/or deformation mechanisms in addition to dislocation creep. We will discuss these aspects below.

6.2.1. Grain size stabilization

In terms of the aforementioned balance between grain growth and reduction it is important to note that both the median grain size and the width of the grain size distribution increase in a non-linear way with temperature (Figs. 4 and 6). A comparison with previous studies on carbonate mylonites reveals that the observed trend seems to be of general validity for mid-crustal shear zones in calcite rocks, though considerable scatter exists in the literature data (Fig. 12a). The scatter might result from uncertainties in temperature estimations, differences in strain rates for the different locations investigated and variations in the purity of the carbonate (trace elements: Freund et al., 2004; nano-scale particles: Herwegh and Kunze, 2002; micron-scale particles: Herwegh and Berger, 2004), and therefore emphasizes the importance of microstructural studies that focus on large-scale structures with similar deformation history but variable temperature gradient (see also Dunlap et al., 1997; Stipp et al., 2002). Steady state grain sizes were also obtained for Carrara marble deformed in high strain torsion experiments (Pieri et al., 2001; Barnhoorn et al., 2004). In these experiments a steadily increasing steady state grain size with temperature is manifest (Fig. 12b). Extrapolation of this trend towards our natural samples would fit reasonably with the natural low temperature mylonite but would fail at higher temperatures because of a more pronounced increase with temperature in nature. Concentrating on the concept of grain size stabilization by competing grain size reducing mechanisms and grain growth in the mylonites, the change in grain size with temperature/stress suggests a change in the contributions of the individual grain size modification processes with temperature/stress, such that the growth component increased relative to the grain size reduction/nucleation component, a fact which is not observed in the aforementioned experiments. With respect to an enhanced syndeformational growth component, two potential driving forces have to be considered. First, the grain boundary mobility can be increased by enhanced internally stored (i.e. defect-related) energy. However, it is unclear if this will induce an increase in growth rate or just accelerate dynamic recrystallization such that less time is required for an incremental dynamic recovery of the aggregate. Second, grain growth particularly for small grain sizes might have been largely driven by surface energy. It is striking in this respect that the change in slope of the relationship of grain size versus inverse temperature (Fig. 12c) coincides with the onset of static grain growth in calcite marbles observed in the contact aureole of the Adamello pluton (see Herwegh and Berger, 2003). We tentatively use this correspondence as evidence for an increased contribution of grain growth to the grain size stabilization process in our samples from this temperature onwards. Moreover, the grain size increases with similar slope as in the static (Adamello) case at higher temperatures (Fig. 12c). In the static case, Herwegh and Berger (2003) suggested that this growth was closely related to the presence of fluids, which were generated by decay of organic matter under the presence of water. As evident by the continuous formation of syndeformational calcite veins (see above), enhanced mass transfer under the presence of fluids must also be considered for the development of the steady state microstructures in the present samples. This inference is further supported by the aforementioned temperature-dependent increase in size of sheet silicates (Fig. 13), which occur as second phases within the calcite mylonites. Interestingly, the grain coarsening of the second phases in the shear zone is much more pronounced than in the hanging wall. Hence, deformation enhanced mass transfer along grain boundaries of the matrix calcite took place, promoting the sheet silicates as a marker system for diffusion/mass transfer processes. The presence of fluids would explain the observed discrepancy between nature and experiments. Alternatively, different activation energies for grain growth and grain size reduction mechanisms would yield different relative contributions of the two competing processes and therefore to microstructural differences between nature and experiment.

6.2.2. Grain elongation and SPO

With increasing temperature, we observed an increase in grain elongation (lower *b*/*a* value; Fig 8) and a small decrease in SPO orientation with respect to the shear plane (Table 1). Associated with the increase in grain elongation, the calculated grain surface area per grain increased (Fig. 8). This observation excludes a pronounced effect of static annealing because, in that case, more equidimensional grains would have been expected the warmer the samples were. However, the opposite is the case in the samples investigated. The observed increase in grain elongation could simply be due to increased activity of intracrystalline mechanisms with temperature, but alternatively anisotropic grain growth involving heterogeneous diffusion of matter would have had a similar influence (see Karato and Masuda, 1989). In the case of enhanced intracrystalline plasticity, a change in CPO intensity is expected, which, however, has not been observed (Fig. 9). Hence, increasing anisotropic

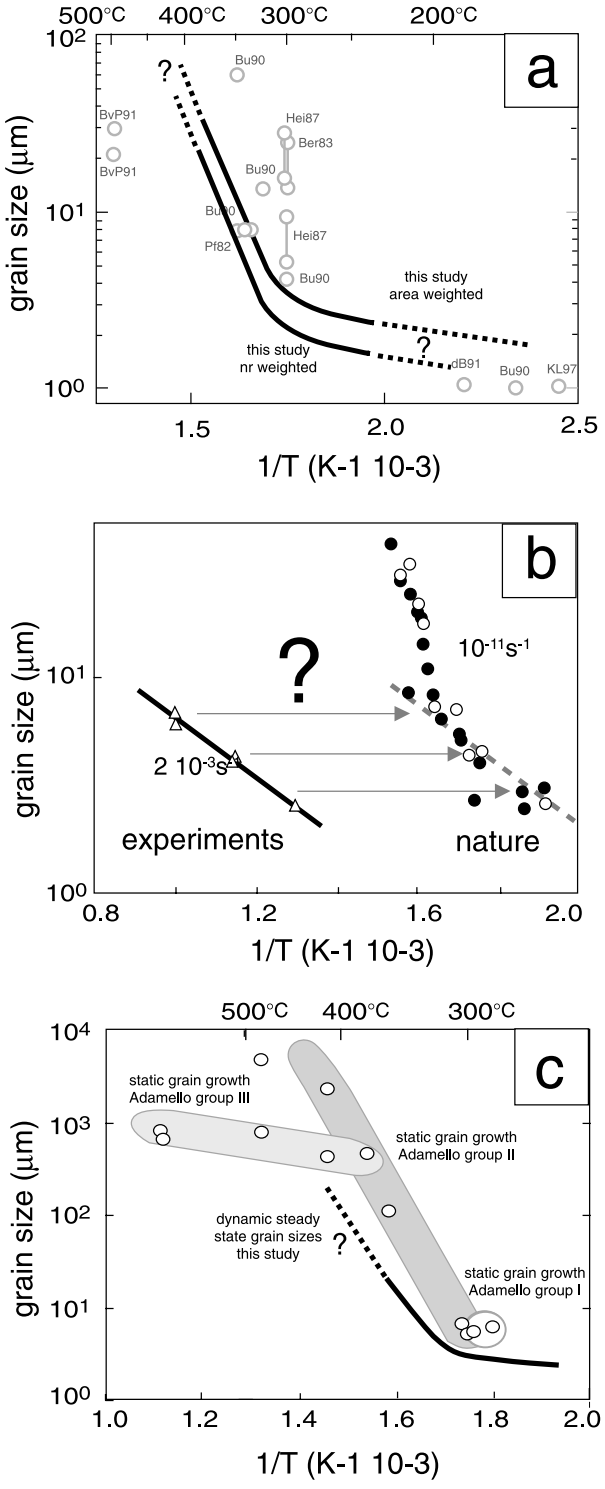

Fig. 12. (a) Compilation of steady state grain sizes of natural calcite mylonites for different deformation temperatures (Ber: Behrmann, 1983; Bu: Burkhard, 1990; BvP: Busch and van der Pluijm, 1995; dB: de Bresser, 1991; Hei: Heitzmann, 1987; KL: Kennedy and Logan, 1997; Pf: Pfiffner, 1982). (b) Comparison between experimentally derived steady state grain sizes obtained by high strain torsion experiments (Pieri et al., 2001; Barnhoorn et al., 2004) and the natural ones of this study. (c) Comparison between changes in grain size as a function of temperature for static grain growth (Herwegh and Berger, 2003) and deformation conditions of this study.

grain growth appears to be the better candidate to explain the gradual change in grain elongation with temperature. An important consequence of this is that grain elongation should not be used as an indicator of the importance of dislocation mechanisms. Differently stated, more equidimensional shapes of grains do not (necessarily) imply a higher contribution of grain size sensitive deformation mechanisms. In addition, if anisotropic grain growth becomes more important the time required for complete reworking of the microstructure is likely to have been expanded, or in other words, slower growth-reduction recrystallization cycles will have resulted. Support for such slow cycles comes from the observations on a rock analogue material and from calcite experiments. High strain simple shear experiments on norcamphor (Herwegh and Handy, 1998) and calcite (Pieri et al., 2001) at high homologous temperatures showed typical SPO orientations of 60° with respect to the shear plane, i.e. far higher than found in our natural samples. With decreasing homologous temperature, however, Barnhoorn et al. (2004) demonstrated that the orientation of the SPO in experimentally deformed calcite rocks is substantially lower, in the order of 20°. These authors suggest that the low angle resulted from slower cycles of recrystallization, an interpretation that is consistent with our inferences for the natural samples.

6.2.3. CPO

We can compare our natural CPO's with experimentally obtained patterns. High-strain experiments of Barnhoorn et al. (2004) showed typical c-axis point maxima perpendicular to the shear plane, roughly comparable with our measurements (cf. their fig. 10 with Fig. 9 of this study). At lower temperature (Barnhoorn et al., 2004), the c-axis point maxima are far less clear, but a-axes smeared out along a great circle subparallel to the shear plane are common. This type of a-axes distribution has also been noted in our natural samples (fig. 6 in Herwegh and Kunze, 2002), but only together with strong c-axis maxima. These discrepancies between nature and experiment may well

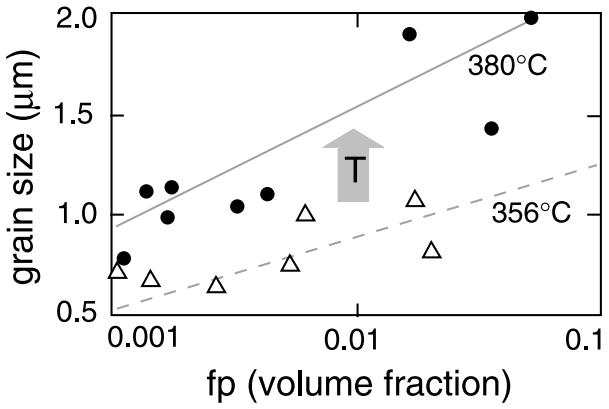

Fig. 13. Volume fraction of second phases (sheet silicates) versus their grain size for samples deformed at 356 and 380 °C. Note increase of grain size with temperature for constant volume fraction.

indicate differences in the relative contributions of different mechanisms during preservation of steady state microfabrics requiring information about the rates of individual processes and their changes with temperature, stress and strain rate in future experimental studies.

In summary, many microstructural observations suggest mass transfer processes/diffusion to have played an increasingly important role in the microstructural reworking of our samples towards higher temperature, in particular in governing (anisotropic) grain growth. Further, changes in microstructure with rising temperature (e.g. grain elongation) appear not to be related to enhanced activity of dislocation mechanisms (no change in CPO strength). Hence, mass transfer/diffusion mechanisms appear to gradually obtain a more prominent role in the steady state deformation of our natural calcite samples towards higher temperature. Unfortunately, quantification of the relative importance of dislocation and diffusion mechanisms solely on the basis of microstructural features such as grain elongation and CPO strength is not possible. Although high strain experiments also induce dynamic steady state microfabrics, considerable microstructural and textural differences prevent a direct correlation between nature and experiment. For that reason, we compare in the following section the rheology modeling using composite flow laws with the microstructural inferences.

6.3. Microstructures vs. composite rheology

The results of our calculations on composite GSI + GSS creep as a function of temperature show that if single mean values for the grain size are used, no trend in relative contribution of deformation mechanisms emerges (Fig. 10). This is inconsistent with the systematic changes in microstructures of the deformed mylonites from the Helvetic Nappe stack with increasing temperature at constant strain rate (Figs. 6–8). In contrast, calculations applying grain size distributions (Fig. 11) result in a general trend of increasing %GSS of total with increasing temperature. We conclude that rheological modeling using experimentally calibrated flow laws is best performed taking into account full grain size distributions, rather than representing grain size by single mean values.

Strain rates in the order of 10^{-11}–10^{-10} s^{-1} were estimated to apply to our natural samples (Section 3.4). Our calculations using the Walker et al. (1990) flow law for GSS creep predict that the calcite mylonites dominantly to almost exclusively deformed by GSS mechanisms at the higher temperatures (at $T > 340$ °C at 10^{-10} s^{-1} and $T > 300$ °C at 10^{-11} s^{-1}; Fig. 11). Although we were not able to exactly quantify the relative contribution of GSS and GSI on the basis of the microstructures of our samples, it is clear that dislocation (GSI) mechanisms played a very important role at all temperatures (e.g. Fig. 9). Consequently, the Walker et al. (1990) flow law predicts mechanical behavior not fully consistent with the microstructural observations. The application of the Herwegh et al. (2003) rate equation for GSS creep, on the other hand, predicts combined GSS + GSI creep dominated by GSI-mechanisms for almost all samples (Fig. 11). With increasing T, the contribution of GSS-mechanisms increased, but generally remained below 60%, in particular if strain rate was more towards 10^{-10} than 10^{-11} s^{-1}. In this sense the modeling approach independently confirms the strain rates obtained by geologic constraints (see above). As discussed above, the microstructures suggest an increased contribution of mass transfer/diffusion processes to the microstructure development. The rheology calculations using the Herwegh et al. (2003) GSS equation, constrained by estimated natural strain rates, are consistent with this. The rheological modeling performed in this study presents a possible way out of the so far existing calcite dilemma, i.e. the discrepancy between deformation mechanisms inferred from natural microstructures and deformation mechanisms predicted by extrapolated experiment-based deformation mechanism maps. The calculations thereby provide a means to quantify relative contributions of mechanisms and conditions of deformation for natural rocks with complex microstructures, i.e. for conditions that cannot be covered by experiments alone. We note that the natural conditions applicable to the field area under study are representative for most upper- to mid-crustal carbonate shear zones (e.g. de Bresser et al., 2002; see also Fig. 12a) and therefore the results are of general validity.

It was noted previously that grain elongation increased with increasing temperature (Fig. 7). Concurrently with this, the %GSS of total went up. Using (a) the lack of trend in CPO strength with temperature, (b) the change in grain size with temperature, and (c) the evidence for increasing mass transfer with temperature, we argued above that this gradual change in elongation is more likely to be related to anisotropic grain growth than to enhanced dislocation activity, in agreement with the calculated rheology of the rocks (i.e. the increasing %GSS to total).

6.4. Paleopiezometry

The recrystallized grain sizes measured in the samples from the Helvetic Nappe stack can be used to determine paleostresses using the piezometric relations of Rutter (1995). Resulting values vary from ~100 MPa at $T =$ 380 °C to 1000 MPa or higher at $T < 250$ °C (Fig. 14). Note that the calcite piezometer of Schmid et al. (1980) give similar results as the rotation recrystallization piezometer from Rutter (1995). Based on the large-scale tectonic setting an overburden of about 10–15 km is realistic, suggesting lithostatic pressures in the range of 300–400 MPa. Thus, for a large part, these stresses lay above the lithostatic pressure and are therefore unrealistically high. The rheology modeling of composite GSS + GSI creep allows for an alternative approach. Added to Fig. 14 are stress values for GSS + GSI creep for a realistic natural strain rate of

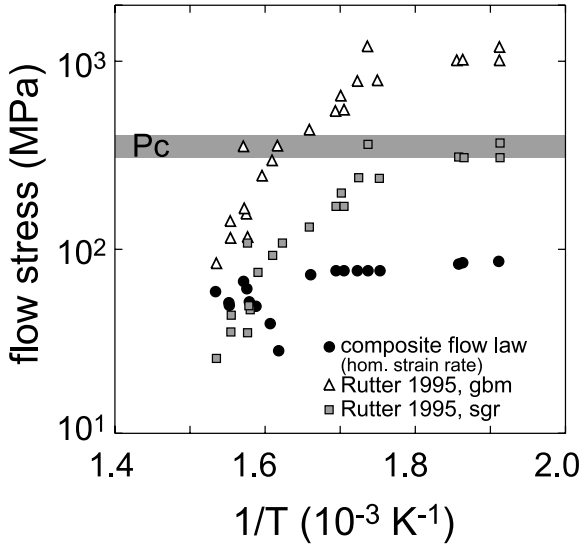

Fig. 14. Comparison between stresses obtained via the recrystallized grain size piezometric relations of Rutter (1995) for grain boundary migration (gbm) and progressive subgrain rotation (sgr), and values resulting from the composite flow law approach (homogeneous stress) of this study. Stress values calculated for homogeneous strain rate would overlap with homogeneous stress data for most values and are left out of the diagram. Pc refers to the lithostatic pressure relevant for the samples.

10^{-11} s^{-1}, using the Herwegh et al. (2003) flow law for GSS creep including full grain size distributions. Stress values are below 100 MPa and slightly decrease with increasing temperature. These magnitudes appear more realistic for the current deformation conditions than the values coming out of the classical recrystallized grain size piezometer. The difference between the piezometer and the flow law approach becomes less if temperatures are high (see also de Bresser et al., 2002).

The data of Fig. 14 demonstrate a discrepancy between stress estimates resulting from piezometric relations and those coming from flow laws, which seems inconsistent given that both piezometer and flow law were calibrated on the basis of largely the same experimental measurements. However, most piezometric relations available for rock materials, including those for calcite, are fully empirical, hence defined independent of flow law parameters and are strictly only applicable at the experimental conditions they were calibrated for. The larger the difference between experimental and natural conditions, the larger the error associated with the application of the empirical piezometric relation. Hence, large deviations may be expected between piezometer and flow law predictions.

7. Conclusions

We studied low-grade calcite mylonite samples from thrust planes in the Helvetic Nappe stack, Switzerland, with the aim to test the hypothesis that composite behavior of grain size insensitive (GSI) dislocation creep and grain size sensitive (GSS) diffusion creep constrained by quantified microstructural parameters can explain the apparent discrepancy between natural observations on deformed calcite rocks and predictions based on deformation experiments.

The following is concluded:

- Grain microstructures of the mylonites represent a steady state balance between grain size reduction and grain growth, evidenced by grain modifications of originally fine-grained micritic limestones and coarse-grained cross-cutting synkinematic veins.
- With increasing temperature along the thrust planes, grain size, grain size distribution, grain elongation, orientation of grain long axis (SPO) and grain surface change in a systematic way. In contrast, crystallographic preferred (c-axis) orientations (CPO) remain of similar strength. These observations indicate enhanced mass transfer/diffusion processes towards higher temperature rather than increased activity of dislocation creep mechanisms. Single dominant creep mechanisms cannot explain the observed trends in microstructure modification.
- Calculations of composite creep behavior using experimentally calibrated flow laws for GSI and GSS of calcite only produce meaningful results if full grain size distributions are included. With increasing temperature, an increased contribution of GSS mechanisms to the overall creep rate followed from the modeling.
- Estimates of creep behavior and characteristics of the microstructure can only be reconciled if strain rates were in the order of 10^{-10}–10^{-11} s^{-1}. Independent constraints on strain rates are in excellent agreement with the predicted values.
- Grain elongation or equidimensionality is not a good microstructural parameter to infer relative importance of GSI or GSS.
- On the basis of the composite creep behavior inferred for the natural calcite rocks, we estimated paleostresses during deformation to be in the order of 80–100 MPa. Application of available recrystallized grain size piezometric relations produced unrealistically high values, notably at the lower temperature. Hence, the calcite grain size piezometers at present cannot be applied with confidence to low T conditions.

Acknowledgements

Susanne Buiter is gratefully acknowledged for calculating the plate convergence rates. The manuscript benefited from the thorough and encouraging reviews of M. Burkhard and L. Kennedy. M. Herwegh acknowledges financial support by SNF (Project 21-66889.01).

References

Adams, B.L., Wright, S.I., Kunze, K., 1993. Orientation imaging—the emergence of a new microscopy. Metallurgical Transactions A 24, 819–831.

Anovitz, L.M., Essene, E.J., 1987. Phase equilibria in the system $CaCO_3$–$MgCO_3$–$FeCO_3$. Journal of Petrology 28, 389–414.

Arkai, P., Ferreiro Mählmann, R., Suchy, V., Balogh, K., Sykorova, I., Frey, M., 2002. Possible effects of tectonic shear strain on phyllosilicates: a case study from the Kandersteg area, Helvetic domain, Central Alps, Switzerland. Schweizerische Mineralogische und Petrographische Mitteilungen 82, 273–290.

Badertscher, N.P., Burkhard, M., 2000. Brittle–ductile deformation in the Glarus Lochseiten (LK) calc-mylonite. Terra Nova 12, 281–288.

Barnhoorn, A., Bystricky, M., Kunze, K., Burlini, L., 2004. The role of recrystallization on the deformation behavior of calcite rocks: high strain torsion experiments on Carrara marble. Journal of Structural Geology 16, 885–903.

Behrmann, J.H., 1983. Microstructure and fabric transitions in calcite tectonites from Sierra Alhamilla (Spain). Geologische Rundschau 72, 605–618.

Bestmann, M., Prior, D.J., 2003. Intragranular dynamic recrystallization in naturally deformed calcite marble: diffusion accommodated grain boundary sliding as a result of subgrain rotation recrystallization. Journal of Structural Geology 25, 1597–1613.

Bestmann, M., Kunze, K., Matthews, A., 2000. Evolution of a calcite marble shear zone complex on Thassos Island, Greece: microstructural and textural fabrics and their kinematic significance. Journal of Structural Geology 22, 1789–1807.

Brodie, K.H., Rutter, E.H., 2000. Deformation mechanisms and rheology: why marble is weaker than quartzite. Journal of the Geological Society, London 157, 1093–1096.

Burkhard, M., 1988. L'Helvetique de la bordure occidentale du massif de l'Aar (évolution tectonique et métamorphique). Eclogae geologicae Helvetiae 81, 63–114.

Burkhard, M., 1990. Ductile deformation mechanisms in micritic limestones naturally deformed at low temperatures (150–350 °C), in: Knipe, R.J., Rutter, E.H. (Eds.), Deformation Mechanisms, Rheology and Tectonics Geological Society, London, Special Publication, 54, pp. 241–257.

Burkhard, M., Kalkreuth, W., 1989. Coalification in the northern Wildhorn nappe and adjacent units, Western Switzerland. Implications for tectonic burial histories. International Journal of Coal 11, 47–64.

Busch, J.P., van der Pluijm, B.A., 1995. Calcite textures, microstructures and rheological properties of marbles in the Bancroft shear zone, Ontario, Canada. Journal of Structural Geology 17, 677–688.

Caciagli, N.C., Manning, C.E., 2003. The solubility of calcite in water at 6–16 kbar and 500–800 °C. Contributions to Mineralogy and Petrology 146, 275–285.

de Bresser, J.H.P., 1991. Intracrystalline deformation of calcite. Geologica Ultraiectina 79. PhD thesis, Utrecht University, The Netherlands.

de Bresser, J.H.P., 2002. On the mechanism of dislocation creep of calcite at high temperature: inferences from experimentally measured pressure sensitivity and strain rate sensitivity of flow stress. Journal of Geophysical Research 107, B12, 2337, DOI:10.1029/2002JB0011812.

de Bresser, J.H.P., ter Heege, J.H., Spiers, C.J. 2001. Grain size reduction by dynamic recrystallization: can it result in major rheological weakening? International Journal of Earth Sciences (Geologische Rundschau) 90, 28–45.

de Bresser, J.H.P., Evans, B., Renner, J., 2002. Predicting the strength of calcite rocks under natural conditions, in: de Meer, S., Drury, M.R., de Bresser, J.H.P., Pennock, G.M. (Eds.), Deformation Mechanisms, Rheology and Tectonics: Current Status and Future Perspectives Geological Society, London, Special Publications, 200, pp. 309–329.

Dietrich, D., Song, H., 1984. Calcite fabrics in a natural shear environment, the Helvetic nappes of western Switzerland. Journal of Structural Geology 6, 19–32.

Dunlap, W.J., Hirth, G., Teyssier, C., 1997. Thermomechanical evolution of a ductile duplex. Tectonics 16, 983–1000.

Exner, H.E., 1972. Analysis of grain- and particle-size distributions in metallic materials. International Metallurgy Reviews 17, 25–42.

Freeman, B., Ferguson, C.C., 1986. Deformation mechanism maps and micromechanics of rocks with distributed grain sizes. Journal of Geophysical Research 91, 3849–3860.

Freund, D., Wang, Z., Rybacki, E., Dressen, G., 2004. High-temperature creep of synthetic calcite aggregates: influence of Mn-content. Earth and Planetary Science Letters, in press.

Frey, M., Robinson, D., 1999. Low-Grade Metamorphism. Blackwell Science Ltd.

Frey, M., Teichmüller, M., Teichmüller, R., Mullis, J., Künzi, B., Breitschmid, A., Gruner, U., Schwizer, B., 1980. Very low grade metamorphism in external parts of the Central Alps: Illite crystallinity, coal rank and fluid inclusion data. Eclogae geologicae Helvetiae 73, 173–203.

Fueten, F., 1997. A computer-controlled rotating polarizer stage for the petrographic microscope. Computers and Geosciences 2, 203–208.

Fueten, F., Hynes, K., Van Luttikhuisen, R.L., 2002. An experimental setup for analysis of analogue deformation experiments using the rotating polariser stage. Journal of Structural Geology 24, 241–245.

Handy, M.R., 1990. The solid-state flow of polymineralic rocks. Journal of Geophysical Research 95, 8647–8661.

Handy, M.R., 1994. Flow laws for rocks containing two non-linear viscous phases: a phenomenological approach. Journal of Structural Geology 16, 287–301.

Heilbronner, R., Bruhn, D., 1998. The influence of three-dimensional grain size distributions on the rheology of polyphase rocks. Journal of Structural Geology 20, 695–707.

Heitzmann, P., 1987. Calcite mylonites in the Central Alpine 'root zone'. Tectonophysics 135, 207–215.

Herwegh, M., 2000. A new technique to automatically quantify microstructures of fine grained carbonate mylonites: two step etching combined with SEM imaging and image analysis. Journal of Structural Geology 22, 391–400.

Herwegh, M., Berger, A., 2003. Differences in grain growth of calcite: a field-based modeling approach. Contributions to Mineralogy and Petrology 145, 600–611.

Herwegh, M., Berger, A., 2004. Deformation mechanisms in Zener dragged systems and their microstructural energy balance. Journal of Structural Geology 26, 1483–1498.

Herwegh, M., Handy, M.R., 1998. The origin of shape preferred orientation in mylonite: inferences from in-situ experiments on polycrystalline norcamphor. Journal of Structural Geology 20, 681–694.

Herwegh, M., Jenni, A., 2001. Granular flow in polymineralic rocks bearing sheet silicates: new evidences from natural examples. Tectonophysics 332, 309–320.

Herwegh, M., Kunze, K., 2002. The influence of nano-scale second phase particles on deformation of fine grained calcite mylonites. Journal of Structural Geology 24, 1463–1478.

Herwegh, M., Handy, M.R., Heilbronner, R., 1997. Temperature and strain rate dependent microfabric evolution in monomineralic mylonite: evidence from in situ deformation of a rock analogue. Tectonophysics 280, 83–106.

Herwegh, M., Xiao, X., Evans, B., 2003. The effect of dissolved magnesium on diffusion creep in calcite. Earth and Planetary Science Letters 212, 457–470.

Higgins, M.D., 2000. Measurement of crystal size distributions. American Mineralogist 85, 1105–1116.

Huon, S., Burkhard, M., Hunziker, J.-C., 1994. Mineralogical, K–Ar, stable and Sr isotope systematics of K-white micas during very low-grade metamorphism of limestones (Helvetic nappes, western Switzerland). Chemical Geology 113, 347–376.

Karato, S., 1989. Grain growth kinetics in olivine aggregates. Tectonophysics 168, 255–273.

Karato, S., Masuda, T., 1989. Anisotropic grain growth in quartz aggregates under stress and its implication for foliation development. Geology 17, 695–698.

Kennedy, L.A., Logan, J.M., 1997. The role of veining and dissolution in the evolution of fine-grained mylonites: the McConnell thrust, Alberta. Journal of Structural Geology 19, 785–797.

Kennedy, L.A., White, J.C., 2001. Low-temperature recrystallization in calcite; mechanisms and consequences. Geology 29, 1027–1030.

Kirschner, D.L., Cosca, M.A., Masson, H., Hunziker, J.C., 1996. Staircase $^{40}Ar/^{39}Ar$ spectra of fine-grained white mica: timing and duration of deformation and empirical constraints on argon diffusion. Geology 24, 747–750.

Lafrance, B., White, J.C., Williams, P.F., 1994. Natural calcite c-axis fabrics: an alternate interpretation. Tectonophysics 229, 1–18.

Means, W.D., 1981. The concept of steady-state foliation. Tectonophysics 78, 179–199.

Molli, G., Conti, P., Giorgetti, G., Meccheri, M., Oesterling, N., 2000. Microfabric study on the deformational and thermal history of the Alpi Apuane marbles (Carrara marbles), Italy. Journal of Structural Geology 22, 1809–1825.

Panozzo, R., 1983. Two-dimensional analysis of shape-fabric using projections of digitized lines in a plane. Tectonophysics 95, 279–294.

Panozzo, R., Hürlimann, H., 1983. A simple method for the quantitative discrimination of convex and convex–concave lines. Microscopica Acta 87, 169–176.

Panozzo, R., Heilbronner, R., Pauli, C., 1994. Orientation and misorientation imaging: integration of microstructural and textural analysis, in: Bunge, H.J., Siegesmund, S., Skrotzki, W., Weber, K. (Eds), Textures of Geological Materials, DGM, pp. 147–164.

Paterson, M.S., 2001. Relating experimental and geological rheology. International Journal of Earth Sciences (Geologische Rundschau) 90, 157–167.

Pfiffner, A.O., 1982. Deformation mechanisms and flow regimes in limestone from the Helvetic zone of the Swiss Alps. Journal of Structural Geology 4, 429–442.

Pfiffner, O.A., Ramsay, J.G., 1982. Constraints on geological strain rates: arguments from finite strain states of naturally deformed rocks. Journal of Geophysical Research 87, 311–321.

Pfiffner, O.A., Lehner, P., Heitzmann, P., Mueller, S., Steck, A., 1997. Deep Structure of the Swiss Alps. Birkhäuser.

Pieri, M., Burlini, L., Kunze, K., Stretton, I., Olgaard, D.L., 2001. Rheological and microstructural evolution of Carrara marble with high shear strain: results from high temperature torsion experiments. Journal of Structural Geology 23, 1393–1413.

Poirier, J.P., 1985. Creep of Crystals. Cambridge University Press.

Raj, R., Ghosh, A.K., 1981. Micromechanical modelling of creep using distributed parameters. Acta Metallica 29, 283–292.

Renner, J., Evans, B., 2002. Do calcite rocks obey the power-law creep equation? in: de Meer, S., Drury, M.R., de Bresser, J.H.P., Pennock, G.M. (Eds.), Deformation Mechanisms, Rheology and Tectonics: Current Status and Future Perspectives Geological Society, London, Special Publications, 200, pp. 293–307.

Renner, J., Evans, B., Siddiqi, G., 2002. Dislocation creep of calcite. Journal of Geophysical Research 107, B12, 2364, DOI: 10.1029/2001JB001680.

Ricou, L.-E., 1994. Thetys reconstructed: plates, continental fragments and their boundaries since 260 Ma from central America to South-eastern Asia. Geodynamica Acta 7, 169–218.

Rosenbaum, G., Lister, G.C., Duboz, C., 2002. Relative motions of Africa, Iberia and Europe during Alpine orogeny. Tectonophysics 359, 117–129.

Royer, J.Y., 1992. A Global Isochron Part. University of Texas Institute for Geophysics.

Ruffini, R., Cosca, M., s'Atri, A., Hunziker, J., 1995. The vulcanic supply of the Taveyanne turbidites (Savoie, France): a riddle for Tertiary Alpine vulcanism. Atti delle Accademia Science Roma 14, 359–376.

Rutter, E.H., 1995. Experimental study of the influence of stress, temperature, and strain on the dynamic recrystallization of Carrara marble. Journal of Geophysical Research 100, 24651–24663.

Schmid, S.M., Paterson, M.S., Boland, J.N., 1980. High temperature flow and dynamic recrystallization in Carrara marble. Tectonophysics 65, 245–280.

Schmid, S.M., Casey, M., Starkey, J., 1981. The microfabric of calcite tectonites from the Helvetic nappes (Swiss Alps), in: McClay, K., Price, N.J. (Eds.), Thrust and Nappe Tectonics Geological Society, London, Special Publications, 9, pp. 151–158.

Schmid, S.M., Panozzo, R., Bauer, S., 1987. Simple shear experiments on calcite rocks: rheology and microfabric. Journal of Structural Geology 9, 747–778.

Shimizu, I., 1998. Stress and temperature dependence of recrystallized grain size: a subgrain misorientation model. Geophysical Research Letters 25, 4237–4240.

Stipp, M., Stünitz, H., Heilbronner, R., Schmid, S.M., 2002. The eastern Tonale fault zone: a 'natural laboratory' for crystal plastic deformation of quartz over a temperature range from 250 to 700 °C. Journal of Structural Geology 24, 1861–1884.

Suchy, V., Frey, M., Wolf, M., 1997. Vitrinite reflectance and shear-induced graphitization in orogenic belts: a case study from the Kandersteg are, Helvetic Alps, Switzerland. International Journal of Coal Geology 34, 1–20.

ter Heege, J.H., 2002. Relationship between dynamic recrystallization, grain size distribution and rheology. Geologica Ultraiectina 218. PhD thesis, Utrecht University, The Netherlands.

ter Heege, J.H., de Bresser, J.H.P., Spiers, C.J., 2002. The influence of dynamic recrystallization on the grain size distribution and rheological behavior of Carrara marble deformed in axial compression, in: de Meer, S., Drury, M.R., de Bresser, J.H.P., Pennock, G.M. (Eds.), Deformation Mechanisms, Rheology and Tectonics: Current Status and Future Perspectives Geological Society, London, Special Publications, 200, pp. 331–353.

ter Heege, J.H., de Bresser, J.H.P., Spiers, C.J., 2004. Composite flow laws for crystalline materials with log-normally distributed grain size: theory and application to olivine. Journal of Structural Geology 26, 1693–1705.

Ulrich, S., Schulmann, K., Casey, M., 2002. Microstructural evolution and rheological behavior of marbles deformed at different crustal levels. Journal of Structural Geology 24, 979–995.

Underwood, E.E., 1970. Quantitative Stereology. Addison Wesley, Reading, Massachusetts.

Van der Pluijm, B.A., 1991. Marble mylonites in the Bancroft shear zone, Ontario, Canada: microstructures and deformation mechanisms. Journal of Structural Geology 13, 1125–1135.

Wager, L.R., 1961. A note on the origin of ophitic texture in the chilled olivine gabro of Skaergaard intrusion. Geological Magazine 81, 1452–1459.

Walker, A.N., Rutter, E.H., Brodie, K.H., 1990. Experimental study of grain-size sensitive flow of synthetic, hot pressed calcite rocks, in: Knipe, R.J., Rutter, E.H. (Eds.), Deformation Mechanisms, Rheology and Tectonics Geological Society, London, Special Publication, 54, pp. 259–284.

Wang, Z., 1994. The effect of grain size distribution on the rheological behavior of polycrystalline materials. Journal of Structural Geology 16, 961–970.